Atmospheric
Measurement
Techniques

Real-world wintertime CO, N₂O, and CO₂ emissions of a central European village

László Haszpra[1,2], **Zoltán Barcza**[3,4,5], **Zita Ferenczi**[6], **Roland Hollós**[3,7,8], **Anikó Kern**[5,9], **and Natascha Kljun**[10]

[1]Institute for Nuclear Research, Debrecen, 4026, Hungary
[2]Institute of Earth Physics and Space Science, Sopron, 9400, Hungary
[3]Department of Meteorology, Institute of Geography and Earth Sciences,
ELTE Eötvös Loránd University, Budapest, 1117, Hungary
[4]Excellence Center, Faculty of Science, ELTE Eötvös Loránd University, Martonvásár, 2462, Hungary
[5]Faculty of Forestry and Wood Sciences, Czech University of Life Sciences Prague, Prague, 165 21, Czech Republic
[6]Hungarian Meteorological Service, Budapest, 1024, Hungary
[7]Centre for Agricultural Research, Agricultural Institute, Martonvásár, 2462, Hungary
[8]Doctoral School of Environmental Sciences, ELTE Eötvös Loránd University, Budapest, 1117, Hungary
[9]Department of Geophysics and Space Sciences, Institute of Geography and Earth Sciences,
ELTE Eötvös Loránd University, Budapest, 1117, Hungary
[10]Centre for Environmental and Climate Science, Lund University, Lund, 223 62, Sweden

Correspondence: László Haszpra (haszpra.l@gmail.com)

Abstract. Although small rural settlements are only minor individual sources of greenhouse gases and air pollution, their high overall occurrence can significantly contribute to the total emissions of a region or country. Emissions from a rural lifestyle may be remarkably different than those of urban and industrialized regions, but nevertheless they have hardly been studied so far. Here, flux measurements at a tall-tower eddy covariance monitoring site and the footprint model FFP are used to determine the real-world wintertime CO, N₂O, and CO₂ emissions of a small village in western Hungary. The recorded emission densities, dominantly resulting from residential heating, are 3.5, 0.043, and 72 µg m⁻² s⁻¹ for CO, N₂O, and CO₂, respectively. While the measured CO and CO₂ emissions are comparable to those calculated using the assumed energy consumption and applying the according emission factors, the nitrous oxide emissions exceed the expected value by a magnitude. This may indicate that the nitrous oxide emissions are significantly underestimated in the emission inventories, and modifications in the methodology of emission calculations are necessary. Using a three-dimensional forward transport model, we further show that, in contrast to the flux measurements, the con-centration measurements at the regional background monitoring site are only insignificantly influenced by the emissions of the nearby village.

1 Introduction

Climate change, primarily caused by the accumulation of greenhouse gases (GHGs) in the atmosphere, is one of the biggest challenges humanity faces. In addition to the direct meteorological consequences, it also manifests in different economical and societal problems including food and water insecurity, migration, political crises, and loss of biodiversity. (IPCC, 2014). For the development of an effective climate change mitigation strategy, we need to know the amount of greenhouse gases emitted by each source. At country level, the emission is calculated based on statistical activity data and emission factors suggested by international guidelines (IPCC, 2019). However, emission inventory guidelines cannot specify emission factors for each activity or all specific conditions and circumstances, resulting in distortion and uncertainty of the officially reported inventory values, which

are the essential input of the European Union's emission control policy. The climatic consequences of anthropogenic GHG emissions depend on the actual amount of GHG emissions rather than the emissions calculated based on potentially uncertain emission factors; therefore, it is highly desirable to validate and improve the accuracy of emission factors. Industrial emissions can be estimated with relatively low uncertainty. Household emissions, however, may vary largely depending on the available infrastructure, socioeconomic conditions, and cultural traditions, especially for small settlements. Although (mega)cities dominate the anthropogenic greenhouse gas emission (Moran et al., 2018), the large number of small settlements with poorly constrained emissions and the scarce direct measurements at village environment scale (Fachinger et al., 2021) contribute to the uncertainty of the estimates of the total anthropogenic emission.

Since 1993, the tall-tower greenhouse gas monitoring station Hegyhátsál has been operated for the Global Atmosphere Watch program of the World Meteorological Organization and the global cooperative air sampling network of the National Oceanic and Atmospheric Administration, USA, in a rural environment in Hungary. In addition to the continuous monitoring of the concentration of direct (CO$_2$, CH$_4$, N$_2$O) and indirect (CO) greenhouse gases, the tower is also equipped with eddy covariance (EC) systems to measure the surface–atmosphere exchange of certain gases. The site is located as far from any major anthropogenic sources as possible in the densely populated central Europe. However, from time to time, the footprint area of the EC systems partly overlaps with the area of a small nearby village (Barcza et al., 2009). There is no industrial or notable commercial activity in the village; therefore, it is an ideal place to estimate one of the most uncertain terms of the emission inventories of small settlements: residential heating. EC measurement-based emission mapping is common in urban environments (see, e.g., Rana et al., 2021, and references herein). In this study, we show that long-term data series at a tall tower can be used for the determination of the emissions of a small settlement occupying only a minor area of the footprint area of the EC system. For the derivation of the residential emissions, the hourly nitrous oxide (N$_2$O), carbon monoxide (CO), and carbon dioxide (CO$_2$) fluxes measured at the tower during the winter seasons (December–February) between December 2015 and February 2021 were used. To the best of our knowledge, we are the first to attempt to apply this technique in a rural, natural environment for the determination of the emission of a village covering only a small part of the footprint area of the measurements.

As footprints of eddy covariance and concentration measurements differ by magnitudes (Gloor et al., 2001; Kljun et al., 2002; Vesala et al., 2008; Barcza et al., 2009), the question arises of whether and to what extent the emissions from the nearby village impact the concentration measurements at the monitoring station. A forward transport model was deployed to answer this question.

2 Methods and measurements

2.1 Basic concept

The eddy covariance (EC) technique is widely used for the determination of the surface–atmosphere flux of atmospheric components within the footprint of the measurements (Franz et al., 2018; Papale, 2020). Although the majority of EC systems are used for the monitoring of gas exchange of different ecological systems, there is a growing number of EC sites used for the estimation of urban anthropogenic emissions (see, e.g., Grimmond et al., 2002; Vogt et al., 2006; Stagakis et al., 2019; Rana et al., 2021). Usually, the emission density in a city is not spatially homogeneous. An appropriate footprint model can help to attribute the measured flux to the emission in specific source areas.

The flux footprint area depends on the measurement height of the EC system and the actual meteorological and surface conditions. Flux footprints of EC measurements performed on a tower almost 100 m tall may cover an area of up to a 100 km^2 (Barcza et al., 2009; Desai et al., 2015; Satar et al., 2016; Chi et al., 2019). Within this area, the village in focus may cover only a few percent. Our concept assumes that, during the winter season, both the "natural" landscape (vegetated area, i.e., agricultural fields, forests) and the built-up area (i.e., the village) are homogeneous from the point of view of emission density. The measured flux (F_{measured}) is then the combination of the fluxes originating from the built-up areas (F_{village}), including the houses, farm buildings, backyards, roads, and parks within the village, and those of the non-residential areas, which we denote here as natural landscape (F_{natural}):

$$F_{\text{measured}} = \alpha \times F_{\text{village}} + (1 - \alpha) \times F_{\text{natural}}, \qquad (1)$$

where α is the contribution of the village within the footprint area. Note that the contribution of the surface flux to the measured flux is not uniform within the footprint area (Schmid, 1994; Kljun et al., 2002; Vesala et al., 2008). The weighted contribution of a surface source at a specific unit area to the measurement at the tower at each time step can be estimated by using the footprint function value at the given point. The integral of the footprint function over the infinite x–y plane equals 1. Hence, with a suitable footprint model, if F_{natural} is known, then F_{village}, the emission density of the village within the footprint area, can be calculated as follows:

$$F_{\text{village}} = (F_{\text{measured}} - (1 - \alpha) \times F_{\text{natural}}) / \alpha. \qquad (2)$$

In a next step, the influence of the emission of the village on the concentration measurements at the monitoring site can be calculated using an appropriate transport model. The realization of this approach requires surface–atmosphere flux measurements, land cover information, and footprint and transport models.

2.2 Monitoring site and instrumentation

The EC measurements used in this study are carried out on a 117 m tall, free-standing TV/radio transmitter tower owned by Antenna Hungária Corp. The tower is located in a fairly flat region of western Hungary, close to the western edge of the Pannonian Basin (46°57′ N, 16°39′ E, 248 m a.s.l.), in the vicinity of the small village called Hegyhátsál, which is the focus of the present study (Fig. 1).

The eddy covariance system is mounted on the tower at 82 m above the ground on an instrument arm of 4.4 m length projecting to the north. The disturbance of the flow pattern during southerly winds is corrected as described in Barcza et al. (2009). The eddy covariance system has been monitoring the vertical flux of CO_2 since 1997 and that of N_2O and CO since 2015. The EC system is based on a GILL R3-50 research ultrasonic anemometer (GILL Instruments Ltd, Lymington, UK), a model 913-0014 enhanced-performance fast-response N_2O / CO / H_2O analyzer (Los Gatos Research Ltd., San Jose, CA, USA) with fast-flow optional accessories, and a model LI-6262 fast-response infrared CO_2 / H_2O analyzer (LI-COR Inc., Lincoln, Nebraska, USA).

In addition to the eddy covariance measurements, the concentration of carbon dioxide and the basic meteorological parameters (wind speed and direction, air temperature, relative humidity) are continuously measured at four elevations along the tower (10, 48, 82, 115 m). In this study, we use the term "concentration" as a synonym of the actually measured "dry mole fraction". For a detailed description of the site and instrumentation see Haszpra et al. (2001, 2018) and Barcza et al. (2020).

2.3 Surface–atmosphere flux calculation

The measurements performed at the tower allow the calculation of the turbulence parameters (vertical wind speed and concentration fluctuations) necessary for the calculation of the vertical fluxes of the substances studied. A detailed description of the methodology for these calculations can be found in Haszpra et al. (2001) and Barcza et al. (2020). The EC system and the data evaluation software provide averaged hourly flux values.

A disadvantage of tall-tower EC systems is that they may be decoupled from the surface by low-level inversions from time to time (Desai et al., 2015; Chi et al., 2019). At our monitoring station, such conditions are especially found during winter. In these situations, the EC systems cannot provide the actual surface–atmosphere flux data. To avoid decoupled measurements in cases of low-level inversion, information on the height of the boundary layer was derived from the ERA5 reanalysis dataset of the European Centre for Medium-Range Weather Forecasts (Copernicus Climate Change Service, 2017) for the grid point nearest the monitoring site with hourly resolution. Taking into account the elevation of the EC system of 82 m above the ground, we re-

moved all flux values from the quality-checked data series (Haszpra et al., 2005, 2018; Barcza et al., 2020) when the top of the boundary layer was below 100 m. Removing these data from the data series, 6371 hourly data points (49.0 % of the total 13 008 winter hours) remained for the study for the six winter seasons (2015/2016–2020/2021) evaluated in this study.

2.4 Environmental and land cover information

The project aims at the determination of the wintertime residential-heating-dominated emissions of Hegyhátsál village. The village is located in the west-to-northwest sector at 400–1200 m of distance from the tower. It has 151 inhabitants in 89 households (Hungarian Central Statistical Office, 2019). There is no industrial or notable commercial activity in the village. Approximately half of the single-family houses of the village are connected to the natural gas distribution network and also use this fuel for heating purposes. The other half of the households use solid fuels for heating. Taking into account the socioeconomic conditions in the region, it is reasonable to assume that heating appliances for biomass or other solid fuels are available and occasionally used even in the households connected to the natural gas network.

The land cover of the region of the monitoring tower consists of a mixture of agricultural fields and small forest patches. In addition to Hegyhátsál, the other neighboring villages are about 3 km away from the tower to the north (Katafa), northwest (Nádasd), and south (Hegyháthodász). The nearest settlement worth mentioning in the eastern sector is Gersekarát, located more than 7 km from the tower (Fig. 1). There is hardly any commercial or industrial activity in this dominantly agricultural region.

The local roads connecting the small settlements carry little traffic (300–600 vehicle units per day). The only major road in the region is the 2 × 1-lane trans-European E65 running northwest–southeast with 4700 vehicle units per day (Magyar Közút, 2019). Its closest point to the monitoring site is about 500 m to the southwest (Fig. 1).

The prevailing wind directions in winter are northeasterly and southwesterly (Fig. 2), although the monitoring station is located in the zone of westerly wind patterns. However, the Alps, rising approximately 100 km to the west of the station, significantly modify the regional wind pattern.

For the identification of the land cover type of the potential source areas of the surface–atmosphere fluxes, the National Ecosystem Base Map of Hungary (NÖSZTÉP) (Tanács et al., 2019) was used. This dataset has 56 categories at level 3 with a spatial resolution of 20 m × 20 m. Within the area of our interest three level-1 NÖSZTÉP categories occur: urban, cropland, and forest. In our study, cropland and forested land cover types are considered natural landscape areas, while the areas labeled as urban (buildings, roads and other artificial surfaces, vegetated areas in an artificial environment – e.g.,
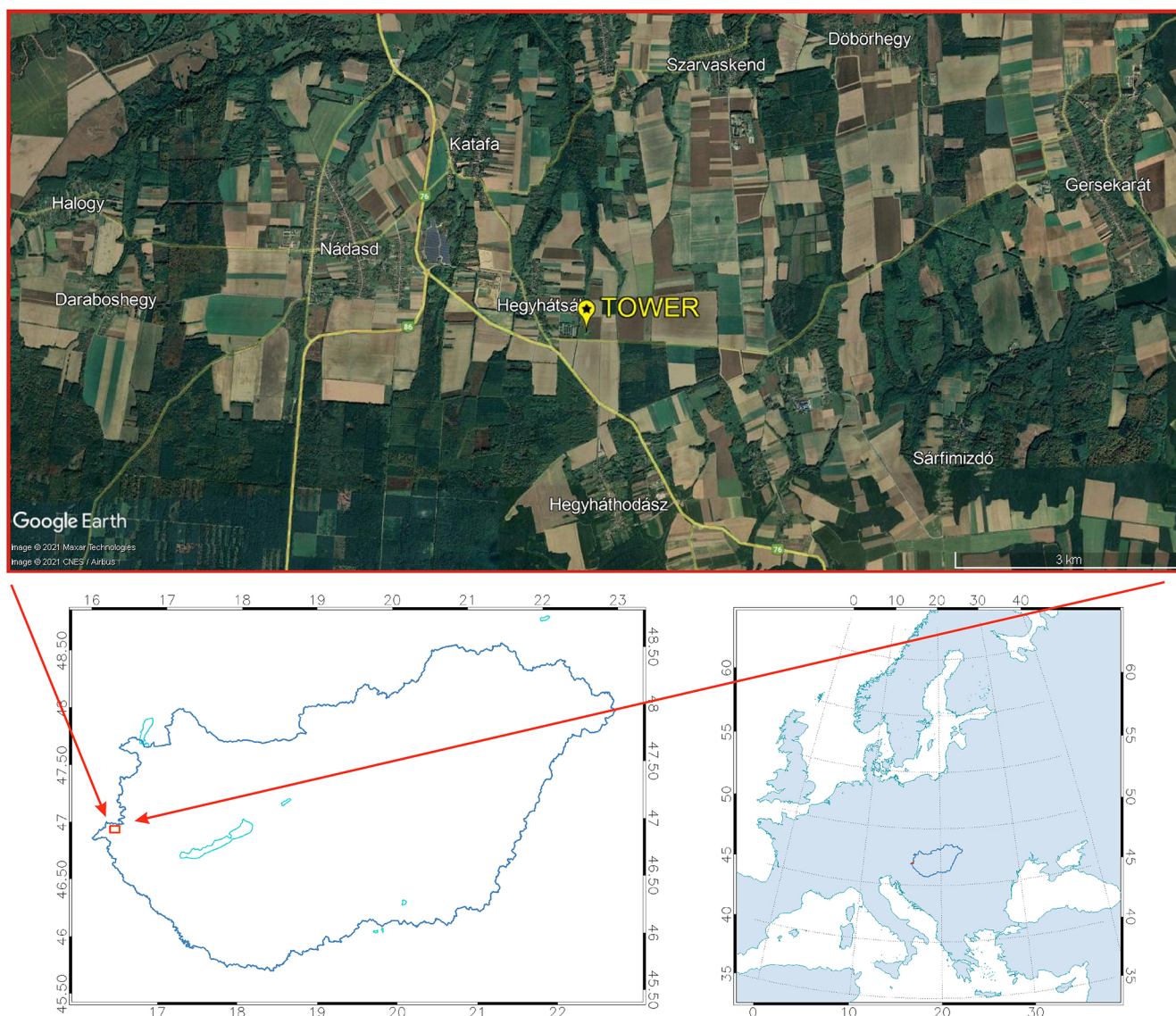
Figure 1. Location and surrounding region of the Hegyhátsál tall-tower GHG monitoring site on a Google Earth satellite image. © Google Earth.

backyards, parks) represent the villages. There are 1645 grid cells covering the area of Hegyhátsál village, which corresponds to its area of 65.8 ha (Fig. 3).

2.5 Footprint model

The flux footprint function is a probability density function describing the relative contribution from each element of the (mainly) upwind surface area source to the measured flux. For the calculation of the source area (footprint) of the flux measurements, the two-dimensional Flux Footprint Prediction (FFP) model of Kljun et al. (2015) has been applied. The model is based on the LPDM-B backward Lagrangian stochastic particle dispersion model valid for a wide range of atmospheric conditions (Kljun et al., 2002, 2004a, b). While

FFP is significantly less resource-intensive than LPDM-B, it is still applicable for stable, neutral, and convective conditions. The model performance was amongst the best in a test of several footprint models against data from a tracer release experiment (Heidbach et al., 2017).

The input parameters of the model are the measurement height above displacement height (z_m), the roughness length (z_0), the Obukhov length (L), the standard deviation of the lateral wind speed (σ_v), the friction velocity (u_*), and the height of the boundary layer (h). The wind direction is an optional input parameter, but it is needed for the geographical localization of the source areas. Displacement height was considered to be negligible due to the lack of vegetation in wintertime (see van der Kwast et al., 2009); thus, the ob-
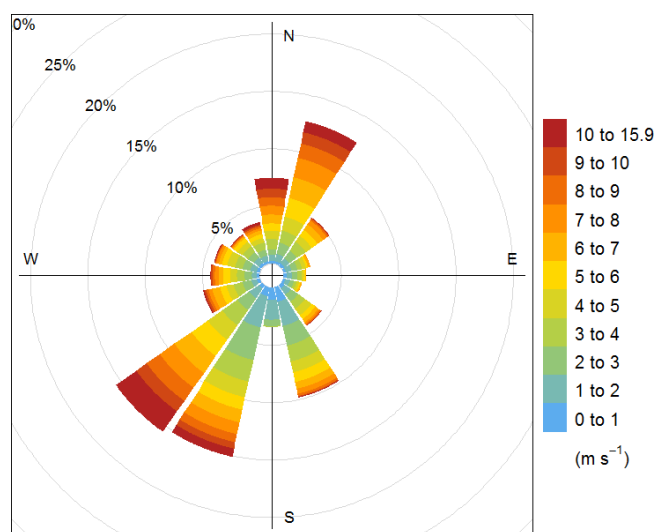
Figure 2. Wintertime (December–February) frequency distribution of wind directions at 82 m height at the Hegyhátsál tall-tower monitoring site between December 2015 and February 2021. The village is located to the northwest of the tower.

Figure 3. Definition of the territory of the village based on land cover information. The shaded area covers the buildings, roads in the village, and vegetated areas in artificial environments (parks, backyards, etc.). © Google Earth.

servation height was used to approximate z_m. The Obukhov length, the standard deviation of the lateral wind speed, the friction velocity, and the wind direction are directly measured or can be calculated from the measurements. The boundary layer height is available from the ERA5 reanalysis dataset (see above) for the region of the tower. The roughness length is assumed to be to equal 0.15 m based on an earlier study (Barcza et al., 2009).

FFP assumes stationarity and horizontal homogeneity of the flow over the time periods of the flux calculations (1 h in our case) and does not include roughness sublayer dispersion near the ground (negligible in this case) or dispersion within the entrainment layer at the top of the convective boundary layer. The scaling parametrization also sets some limitations.

In this study, the model was used with the following restrictions:

$$20z_0 < z_m < h_e, \tag{3}$$

$$-15.5 \leq z_m/L, \tag{4}$$

$$u_* \geq 0.2\,\mathrm{m\,s}^{-1}, \tag{5}$$

where h_e is the height of the entrainment layer. Accepting that typically $h_e \approx 0.8\,h$ (Holtslag and Nieuwstadt, 1986; Kljun et al., 2015), Eq. (3) does not reduce the available flux data as the fluxes measured during $h < 100$ m have already been excluded from the dataset (see above). However, Eqs. (4) and (5) disqualify approximately a third of our measurement data. So, for footprint calculation, 4277 hourly flux data, or 32.9 % of the total winter hours, were available. Theoretically, it is possible to set a lower u_* threshold for the FFP model. However, at low u_* EC systems mounted high above the ground cannot provide the actual surface–atmosphere flux data alone. In such cases, the storage term has to be considered (Haszpra et al., 2005). As the storage term adds considerable uncertainty to the calculated flux due to the noisy signal, it is preferable to avoid low u_* conditions in tall-tower flux derivation.

The discretized footprint function, i.e., the output of the model at the 90 % footprint contribution level, was integrated for each grid cell of the land cover map, giving the contribution of that specific grid cell to the total flux measured at the monitoring site. The footprint function was also integrated over the area of the village (α) to indicate the total contribution of the emission from the village to the measured flux at the monitoring site. To derive α, the integral concerns all grid cells appearing in Fig. 3.

2.6 Transport model

For the estimation of the influence of the emission from the village on the concentration measurements at the monitoring tower, the Graz Lagrangian Model (GRAL v14.8 – Oettl et al., 2002; Oettl, 2015a, b; Romanov et al., 2020) has been used. This 3D particle dispersion model was originally developed for the dispersion of pollutants from a road tunnel portal but is suitable to describe the three-dimensional concentration distribution of area sources. Its input data are wind speed, wind direction, Pasquill–Gifford stability class (determined from the local meteorological measurements), location of the source area relative to the receptor point, and the yield of the source homogeneously distributed over the area. The simulation was run at 10 m horizontal and 3 m vertical resolution for the period of December 2017–February 2018 at 1 h temporal resolution.

3   Results and discussion

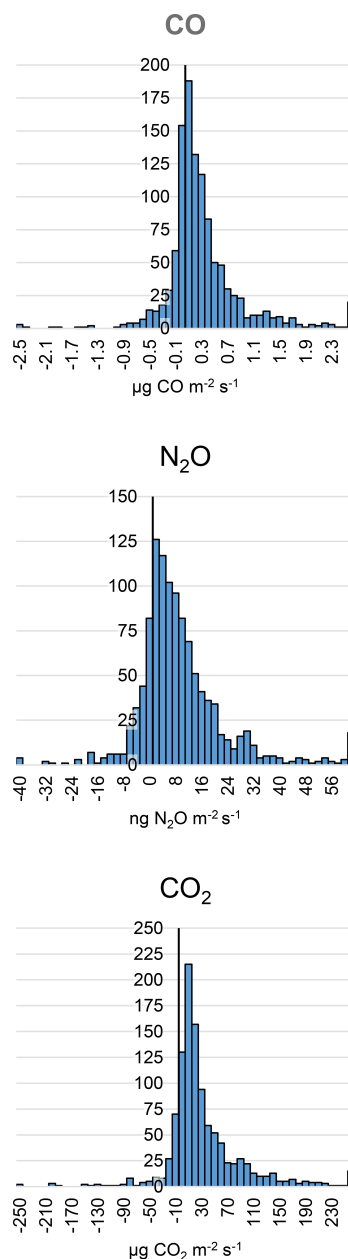## 3.1   Emissions of the natural landscape

The natural sources of carbon monoxide comprise biomass burning, atmospheric oxidation of hydrocarbons, and direct biogenic emissions (Zheng et al., 2019). Open biomass burning (e.g., stubble burning) is prohibited in the study region. Atmospheric oxidation of hydrocarbons requires hydroxyl radicals. Hydroxyl radicals form in photochemical processes, and therefore their concentration is low in the darkest season of the year. The vegetation is dormant in winter, and biogenic emissions also depend on sufficient light (Bruhn et al., 2013). Hence, it can be concluded that natural sources of CO are negligible during wintertime.

The major natural sources of nitrous oxide are denitrification and nitrification processes in soil and water (Tian et al., 2020). These biochemical processes slow down with decreasing temperature (Benoit et al., 2015; Butterbach-Bahl et al., 2013). Nitrogen addition to agricultural soil enhances nitrous oxide emission, which is relevant in our case as the surrounding region of the tower is dominated by croplands (Barcza et al., 2009). Although the average temperature of $+1.6\,°C$ during the study period is rather low for biochemical activities, the croplands (i.e., natural landscape) may emit a detectable amount of N$_2$O.

The net ecosystem exchange of carbon dioxide in the winter season is positive in our region (Haszpra et al., 2005; Barcza et al., 2020); i.e., the landscape is a net source. The dominantly dormant vegetation assimilates only a low amount of carbon dioxide. This process might be temperature-dependent during the winter season. Respiration decreases with decreasing temperature. The result of the two opposing processes of photosynthetic assimilation and respiration creates net emission in winter on average.

For the determination of the emission density of the non-residential landscape (agricultural fields, forests), we selected footprints for which the integrals of the footprint function values over the area of the village (α) were negligible; that is, the emission in the village did not influence the fluxes measured at the monitoring site (at the 90 % footprint contribution level). Obviously, all these 1147 footprints cover areas in the easterly to southerly sector opposite the village Hegyhátsál. To avoid any contamination from remote settlements, data with a footprint peak location farther than 5000 m were excluded from the evaluation, which left us with 1120 footprints and flux data points. Nevertheless, our selection cannot completely exclude any anthropogenic emissions. The local roads with little traffic and small settlements of a few households still contribute to the emission of the natural landscape.

The frequency distribution functions of all measured fluxes are skewed towards positive fluxes with a few extremely high values (Fig. 4). Therefore, instead of the arithmetic average, the emission density of the natural landscape is characterized by the median of the datasets. The medians

Figure 4. Frequency distributions of wintertime natural landscape (agricultural fields, forests) emissions.

are not sensitive to extreme outliers; hence, we did not apply any arbitrary outlier filtering algorithm.

Our method assumes a homogeneous and isotropic spatial distribution of GHG fluxes from the natural landscape. To evaluate whether this condition was met, the measured flux values were grouped into wind sectors of 22.5°, and the median value was calculated for each sector (see Fig. S1 in Supplement). The directional medians were compared with the overall median of the dataset using the asymptotic K-sample Brown–Mood median test. Only the median of the southwest direction deviated significantly ($p < 0.05$) from the overall

Table 1. Emission density of the natural landscape (0 % village coverage) and that of the village calculated at ≥ 25 % and ≥ 30 % footprint-weighted coverage of the village, respectively. n gives the number of footprints available for the calculations. Q25, Q50, and Q75 indicate the lower quartile, the median, and the upper quartile of the emission densities calculated on the basis of the hourly flux values.

Village contribution (%) Number of footprints		0 % ($n = 1120$)	≥ 25 % ($n = 64$)	≥ 30 % ($n = 44$)
CO	Q25	−0.01	1.5	2.1
(μg m^{-2} s^{-1})	Q50	0.14	3.4	3.5
	Q75	0.40	6.0	6.4
N$_2$O	Q25	0.9	8.6	11.6
(ng m^{-2} s^{-1})	Q50	5.9	42.7	42.7
	Q75	13.2	82.5	69.4
CO$_2$	Q25	0	20	7
(μg m^{-2} s^{-1})	Q50	12	86	72
	Q75	42	282	219

median, possibly due to a flux signal from the major road in that direction. Discrimination of a specific direction would have been inconsistent with the otherwise applied α-based filtering. Therefore, we calculated how much the somewhat higher fluxes from this direction contributed to the overall median. For N$_2$O it was 2 %, while for CO and CO$_2$ it was 8 %. These small deviations hardly influence the calculation of the emission from the village. Therefore, to keep the consistency of the filtering method, all available data were used for the calculation of the natural landscape. The sector containing the village could not be tested because of the contribution of the village itself. We hence assumed that the overall median of the natural GHG fluxes was also applicable for this sector.

The emissions of settlements are reported for the average environmental conditions; therefore, the temperature dependence of the natural GHG emissions was not analyzed in depth in this study. For information, Fig. S2 depicts these temperature dependences. Further, due to the diurnal variation in the meteorological conditions, the number of available data was slightly biased towards daytime (Fig. S3). Considering the uncertainty of the data, we do not apply any bias correction in this study.

With the above assumptions, the following emission densities were obtained for CO, N$_2$O, and CO$_2$ for the natural landscape: 139 ng m^{-2} s^{-1}, 5.9 ng m^{-2} s^{-1}, and 12 μg m^{-2} s^{-1}, respectively. Table 1 also lists the lower and upper quartiles of the emission densities to provide an impression of the uncertainty of the median values.
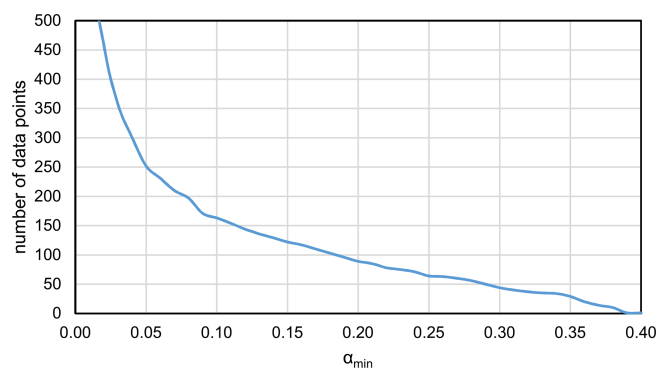

Figure 5. The number of hourly data points when the integral of the footprint function over the village area (α) was greater than or equal to the value indicated on the x axis. At $x = 0$, the total number of data points is included (4277 – outside axis range).

3.2 Emission from the village

For the determination of the emission density of the village using the top-down approach (i.e., estimation of the emission through atmospheric measurements), we should ideally select flux data points when the footprint of the flux measurements exactly covers the area of the village, not missing any part of it and not including anything but the village itself. Due to the location, size, and shape of the village, this was, however, not possible, as all footprints also included non-village contributions. Increasing the required minimum contribution of the village (the integral of the footprint function over the area of the village, α in Eqs. 1 and 2) results in a decrease in the number of available hourly flux data points (Fig. 5). The emission density of the village has been calculated for ≥ 25 % and ≥ 30 % footprint-weighted coverage ($\alpha \geq 0.25$ and $\alpha \geq 0.30$) using the constant $F_{natural}$ and the actual hourly α values in Eq. (2). Figure 6 shows an example of the footprint function with a large α value. In addition to the median flux, Table 1 lists the estimated lower and upper quartiles and the number of footprints available for the calculations. The low number of cases (64 and 44, respectively) is also due to the prevailing wind directions that avoid the village (see Fig. 2). Nevertheless, the small difference between the emission densities derived for ≥ 25 % and ≥ 30 % footprint-weighted coverage indicates that these contributions can be used to satisfactorily derive the emission densities of the village. At ≥ 30 % footprint-weighted coverage, the interquartile ranges are a bit narrower, suggesting slightly lower uncertainty. Figure S4 in the Supplement shows how $F_{village}$ converges as α_{min} increases.

The few data points available for the calculation of $F_{village}$ are concentrated almost exclusively in the daytime period of 09:00–15:00 local standard time (57 of 64 and 42 of 44, respectively), which may distort the calculated emissions. Although there are no quantitative data on the diurnal heating and cooking behavior of the populations, it can be assumed
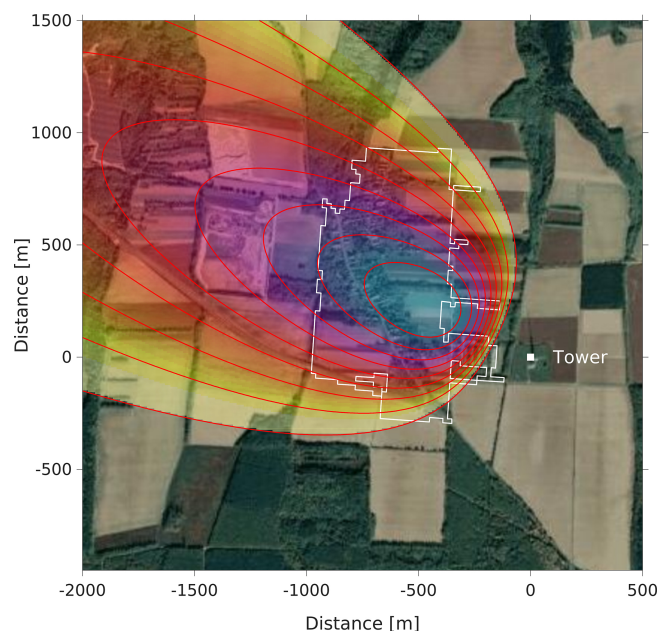
Figure 6. Example of a single flux footprint (10:00–11:00 LST, 27 December 2016). The footprint contour lines (red) show a 10 %–90 % contribution to the flux measurement in 10 % steps. The integral of the footprint function over the village (α, outlined in white) is 0.282 for this case (map source: © Google Earth).

Table 2. Winter season emissions of Hegyhátsál village calculated by applying the top-down (present study) and bottom-up approach, as well as their ratios.

	Top-down (TD) estimation	Bottom-up (BU) estimation	TD / BU
CO	18 Mg	8 Mg	2.2
N₂O	216 kg	8 kg	27
CO₂	364 Mg	310 Mg	1.2

that our data avoid both the nighttime low emission periods as well as the morning and evening high emission periods, and hence they should be representative for the diurnal average emission values. This hypothesis cannot be tested with the available data, and the resulting uncertainty must be taken into account in the interpretation of the results.

The correlation between the air temperature and the top-down emission density of CO, N₂O, and CO₂ is negative and statistically significant at the $p < 0.05$ significance level (-0.369, -0.343, and -0.480, respectively). The negative correlation between the air temperature and the emission supports the fact that the measured flux dominantly originates from residential heating, which is more intensive at low temperatures. This assumption is further supported by the high positive linear correlation ($+0.503$) between CO and CO₂ emissions. As this study provides emissions of the settlement for average environmental winter conditions, we did not discuss the temperature dependence here. For indicative purposes, the temperature dependence of the emission from the village can be found in the Supplement (Fig. S5).

Taking into account the area of the village (65.8 ha) and the median emission densities presented for 30 % coverage in Table 1, the total wintertime (3 months) CO, N₂O, and CO₂ emissions of the village are 17.9, 0.216, and 364 Mg (metric ton), respectively (Table 2).

Alternative emission estimates can be obtained using a bottom-up method, i.e., using published or expert-based emission factors. Most of the buildings in the village are

single-family houses that are several decades old built with traditional brick construction and without insulation. According to expert estimates, such a house of average size may need approximately 57 GJ of energy for winter heating (Gábor Kis-Kovács, Unit of National Emission Inventories, Hungarian Meteorological Service, personal communication, 2021). For the 89 households of the village, this results in approximately 5 TJ during a winter season. As only half of the houses are connected to the natural gas network, a maximum of 2.5 TJ of energy may come from natural gas and a minimum of 2.5 TJ originates from solid fuels, respectively. Liquid fuel is not used for residential heating in Hungary. The default emission factors for natural gas are $26\,\text{kg}\,\text{CO}\,\text{TJ}^{-1}$, $0.1\,\text{kg}\,\text{N}_2\text{O}\,\text{TJ}^{-1}$, and $56.1\,\text{Mg}\,\text{CO}_2\,\text{TJ}^{-1}$, respectively, while for solid fuels they are around $4\,\text{Mg}\,\text{CO}\,\text{TJ}^{-1}$, $4\,\text{kg}\,\text{N}_2\text{O}\,\text{TJ}^{-1}$, and $100\,\text{Mg}\,\text{CO}_2\,\text{TJ}^{-1}$, respectively, depending on the actual fuel type (wood, lignite, etc.) (IPCC, 2006; European Environmental Agency, 2019). Assuming these values, the overall heating emissions are estimated as 10 Mg, 10 kg, and 390 Mg for CO, N₂O, and CO₂, respectively. As it can be assumed that even the households with access to natural gas use some solid fuels for heating, the real emission values may be somewhat higher. In the extreme case, if no natural gas were used at all, the corresponding values would be 20 Mg, 20 kg, and 500 Mg for CO, N₂O, and CO₂.

Under the given climatic conditions, the heating season starts around mid-October and lasts until mid-April. Based on the heating day distribution, 65 %–70 % of the heating energy is used during December–February, i.e., the study period. A conservative estimation of a 10 %–15 % share of solid fuels in the households accessing natural gas would give the approximate emission values of 8 Mg, 8 kg, and 310 Mg for CO, N₂O, and CO₂, respectively, for the December–February period (Table 2).

Although these statistics-based, bottom-up numbers seem to underestimate the CO and CO₂ emissions calculated by the top-down approach – when taking into account the rough estimate of the bottom-up emission and the uncertainties of the top-down approach – the results are similar enough to support the applicability of our method. Our measurements show a higher CO : CO₂ emission ratio (0.049 vs. 0.026), which indicates the contribution of incomplete combustion

that points to biomass rather than natural gas burning. The measurement-based (top-down) N$_2$O emission is 27 times higher than the statistical-based (bottom-up) one. Even if we assume the upper limit of 15 kg TJ^{-1} for the N$_2$O emission factor from solid fuel, the resulting value is still an order of magnitude lower than the measured one. This emission factor may also indicate biomass (or even waste) burning. Our previous study based on concentration measurements (Haszpra et al., 2019) also showed a higher N$_2$O : CO$_2$ ratio compared to the official emission estimates. It suggests that the N$_2$O emission factor for residential heating may be significantly underestimated for the actual conditions. The illegal burning of solid household, municipal, or agricultural waste, which is not rare in villages of poor socioeconomic conditions (Hoffer et al., 2020), may also modify the CO : N$_2$O : CO$_2$ emission ratios. To prove or disprove the presence of waste burning, local measurements of characteristic organics in the atmosphere would be needed.

Although the small sample size implies considerable uncertainty, we tried to estimate if the likely temperature dependence and daily temporal variation of natural emission density ($F_{natural}$) influence the calculated $F_{village}$. For this purpose, the natural fluxes were grouped into 3 h time windows (00:00–03:00, 03:00–06:00, 06:00–09:00 LST), and within each time window the data points were grouped into 3° temperature ranges centrally to 0 °C (−10.5 to −7.5, −7.5 to −4.5, −4.5 to −1.5, −1.5 to +1.5 °C,). The median flux was calculated for each group including at least 10 data points. These median fluxes (Table S1) were used as $F_{natural}$ for the recalculation of $F_{village}$ taking into account the actual temperature and time of the day. The calculated emission densities for CO, N$_2$O, and CO$_2$ from the village at $\alpha \geq 0.3$ are 3.6 µg m^{-2} s^{-1}, 36.3 ng m^{-2} s^{-1}, and 73 µg m^{-2} s^{-1}, respectively, which is practically the same as using the constant $F_{natural}$ (median of the overall dataset). The N$_2$O emission is lower by approximately 15 % according to this method but it does not question the conclusion, namely that the official N$_2$O emission may be significantly underestimated.

### 3.3 Influence of local emissions on the regional background concentration measurements

The Hegyhátsál tall-tower monitoring station is registered in the WMO GAW program (https://gawsis.meteoswiss.ch/GAWSIS/#/search/station/stationReportDetails/0-20008-0-HUN, last access: 21 December 2021) and the ICOS network (https://meta.icos-cp.eu/labeling/, last access: 10 January 2022) as a regional background monitoring site. As such, it should receive as little direct anthropogenic pollution as possible in densely populated, highly industrialized Europe. As the footprints of the eddy covariance measurements (see, e.g., Fig. 6) and those of the concentration measurements (Fig. 7) differ significantly, it is of interest to check by how much the concentration measurements are influenced by the nearby village. We
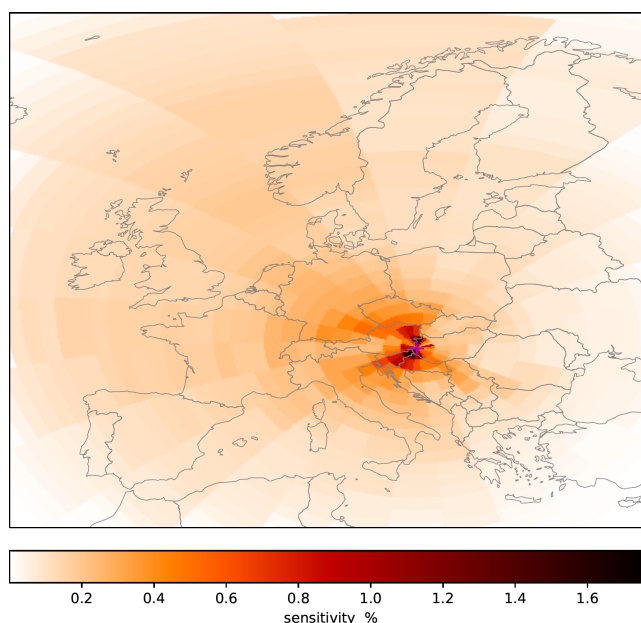
Figure 7. Footprint climatology of the concentration measurements performed at 115 m elevation above the ground in 2019 calculated by the STILT model (Carbon Portal ICOS RI, 2021).

applied the GRAL model for the 2017/2018 winter season to estimate the influence of the village's emissions on the concentration measurements. For the calculations, $F_{village}$ presented in Table 1 for $\alpha \geq 0.3$ was assumed, with a homogeneous distribution over the area of the village. For 1798 h of 2160 h of the study period (83.2 %), emissions from the village did not reach the measurement sensor at all, mainly due to the prevailing wind directions. The prevailing wind directions were northeasterly and southwesterly, while the village is located in the west-northwest sector relative to the measurement tower (see Figs. 2 and 3). In a few cases with winds from west-northwest, i.e., from the village, the pollution could not reach the measurement height at 82 m above the ground due to a shallow boundary layer.

Figure 8 shows the frequency distribution of the excess concentrations derived from the emissions in the village. The excess burden given in mass per volume unit is converted into concentration given in dry mole fraction assuming standard pressure (972 hPa at 248 + 82 m above sea level) and air temperature of +0.6 °C (average over the period of December 2017–February 2018). Due to its high emissions relative to the background concentration, the carbon monoxide concentration is the most sensitive to local pollution. The excess concentration exceeds 2 nmol mol^{-1} in only 0.74 % of the hours. Without considering a specific hour of the study period, the maximum excess was 2.9 nmol mol^{-1}. For comparison, the recommended network compatibility of CO concentration measurements within the scope of the WMO/GAW network is 2 nmol mol^{-1} (WMO, 2020).
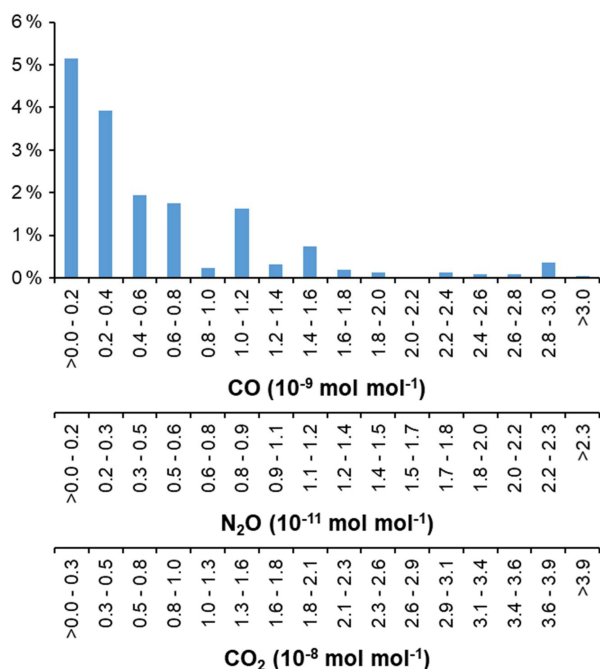
Figure 8. Frequency distribution of the excess concentrations at the measuring point allocated to emission sources in the village. Cases of zero excess (83.2 %) are not presented. The distribution is the same for all components, but the scales are different. Note: scales for N$_2$O and CO$_2$ are rounded and based on the CO scale.

The "hot spot" event mentioned above occurred between 11:00 and 12:00 LT on 4 February when light wind (0.8 m s^{-1}) from the center of the village (wind direction: 300°) directly carried pollution to the measurement sensor in an extremely unstable atmosphere (Pasquill–Gifford stability class A). This process increased the background concentration by 13.6 nmol mol^{-1}. This single-hour measurement has to be highlighted in the quality control process and flagged as a regionally non-representative, locally influenced event.

Carbon dioxide and nitrous oxide behave similarly to carbon monoxide during the short transport time from the village to the tower. Consequently, their excess concentrations caused by the emission in the village are proportional to their emission densities relative to those of carbon monoxide, and the shape of the frequency distributions is the same (Fig. 8). In the case of carbon dioxide, there were only two events (hourly data points) when the excess concentration exceeded 0.04 µmol mol^{-1} (0.06 and 0.18 µmol mol^{-1} in the extreme case discussed above). The values are within the uncertainty of the measurements. Emissions of nitrous oxide were relatively low, causing only a maximum of 0.03 nmol mol^{-1} excess (the extreme value discussed above is 0.10 nmol mol^{-1}), which was practically undetectable.

The wintertime (December–February) average excess of CO, N$_2$O, and CO$_2$ concentrations is 0.10, < 0.01, and 1.34 nmol mol^{-1}, respectively. Due to the lack of industrial

and commercial activities, residential heating is the dominant emission source in the village. This means that the excess concentrations of the village may be even lower in the non-winter seasons. The low values confirm the regional representativeness of the measured concentration data, i.e., that the Hegyhátsál tower qualifies as a regional background monitoring site.

4 Summary and conclusion

In this study, we have shown that tall-tower eddy covariance measurements may be used for the determination of the emission of a smaller region even if it occupies only a minor portion of the footprint area of the measurements. The study is presumably the first one aiming at the direct measurement of GHG emissions of a small rural settlement, while similar measurements have already been performed in urban environments that typically exhibit different emission characteristics. Although the results are subject to significant uncertainties, mainly due to the low number of available data points, the results reveal that while the emission-factor-based calculations of carbon monoxide and carbon dioxide emissions do not differ significantly from the real-world top-down measurements, the emission-factor-based nitrous oxide emission is significantly underestimated. The difference is remarkable and needs explanation even if we consider the uncertainties of both the bottom-up and the top-down calculations presented here. Further in-depth studies are needed, which could potentially result in a correction of the emission factors. The relatively high CO to CO$_2$ ratio and the high N$_2$O emission density suggest a higher than "officially" assumed contribution of biomass burning and a possibility of illegal waste burning.

Using a 3D transport model, we confirmed that the village, as a local pollution source, hardly influences the concentration measurements at the nearby greenhouse gas monitoring station at 82 m height. Hence, the site can be qualified as a regional background monitoring site.

done by ZB. Forward transport modeling was done by ZF. Statistical background calculations were made by RH. Landscape information and processing were handled by AK. Footprint modeling support and editing the paper were conducted by NK. All authors have read and agreed to the published version of the paper.

Disclaimer. Publisher's note: Copernicus Publications remains neutral with regard to jurisdictional claims in published maps and institutional affiliations.

Review statement. This paper was edited by Dominik Brunner and reviewed by two anonymous referees.

References

Barcza, Z., Kern, A., Haszpra, L., and Kljun, N.: Spatial representativeness of tall tower eddy covariance measurements using remote sensing and footprint analysis, Agr. Forest Meteorol., 149, 795–807, https://doi.org/10.1016/j.agrformet.2008.10.021, 2009.

Barcza, Z., Kern, A., Davis, K. J., and Haszpra, L.: Analysis of the 21-years long carbon dioxide flux dataset from a Central European tall tower site, Agr. Forest Meteorol., 290, 108027, https://doi.org/10.1016/j.agrformet.2020.108027, 2020.

Benoit, M., Garnier, J., and Billen, G.: Temperature dependence of nitrous oxide production of a luvisolic soil in batch experiments, Process Biochem., 50, 79–85, https://doi.org/10.1016/j.procbio.2014.10.013, 2015.

Bruhn, D., Albert, K. R., Mikkelsen, T. N., and Ambus, P.: UV-induced carbon monoxide emission from living vegetation, Biogeosciences, 10, 7877–7882, https://doi.org/10.5194/bg-10-7877-2013, 2013.

Butterbach-Bahl, K., Baggs, E. M., Dannenmann, M., Kiese, R., and Zechmeister-Boltenstern, S.: Nitrous oxide emissions from soils: how well do we understand the processes and their controls?, Philos. T. Roy. Soc. B, 368, 20130122, https://doi.org/10.1098/rstb.2013.0122, 2013.

Carbon Portal ICOS RI: STILT station characterization for Hegyhátsál at 115 m, https://hdl.handle.net/11676/F6sSNmtF9qSne9P18HAlusf4, last access: 10 December 2021.

Chi, J., Nilsson, M. B., Kljun, N., Wallerman, J., Fransson, J. E. S., Laudon, H., Lundmark, T., and Peichl, M.: The carbon balance of a managed boreal landscape measured from a tall tower in northern Sweden, Agr. Forest Meteorol., 274, 29–41, https://doi.org/10.1016/j.agrformet.2019.04.010, 2019.

Copernicus Climate Change Service: ERA5: Fifth generation of ECMWF atmospheric reanalyses of the global climate, Copernicus Climate Change Service Climate Data Store (CDS), https://cds.climate.copernicus.eu/cdsapp#!/home (last access: 10 June 2021), 2017.

Desai, A. R., Xu, K., Tian, H., Weishampel, P., Thom, J., Baumann, D., Andrews, A. E., Cook, B. D., King, J. Y., and Kolka, R.: Landscape-level terrestrial methane flux observed from a very tall tower, Agr. Forest Meteorol., 201, 61–75, https://doi.org/10.1016/j.agrformet.2014.10.017, 2015.

European Environmental Agency: EMEP/EEA air pollutant emission inventory guidebook 2019, EEA Report No. 13/2019, ISBN 978-92-9480-098-5, https://doi.org/10.2800/293657, 2019.

Fachinger, F., Drewnick, F., and Borrmann, S.: How villages contribute to their local air quality – The influence of traffic- and biomass combustion-related emissions assessed by mobile mappings of PM and its components, Atmos. Environ., 263, 118648, https://doi.org/10.1016/j.atmosenv.2021.118648, 2021.

Franz, D., Acosta, M., Altimir, N., Arriga, N., Arrouays, D., Aubinet, M., Aurela, M., Ayres, E., López-Ballesteros, A., Barbaste, M., Berveiller, D., Biraud, S., Boukir, H., Brown, T., Brümmer, C., Buchmann, N., Burba, G., Carrara, A., Cescatti, A., Ceschia, E., Clement, R., Cremonese, E., Crill, P., Darenova, E., Dengel, S., D'Odorico, P., Filippa, G., Fleck, S., Fratini, G., Fuß, R., Gielen, B., Gogo, S., Grace, J., Graf, A., Grelle, A., Gross, P., Grünwald, T., Haapanala, S., Hehn, M., Heinesch, B., Heiskanen, J., Herbst, M., Herschlein, C., Hörtnagl, L., Hufkens, K., Ibrom, A., Jolivet, C., Joly, L., Jones, M., Kiese, R., Klemedtsson, L., Kljun, N., Klumpp, K., Kolari, P., Kolle, O., Kowalski, A., Kutsch, W., Laurila, T., de Ligne, A., Linder, S., Lindroth, A., Lohila, A., Longdoz, B., Mammarella, I., Manise, T., Jiménez, S. M., Matteucci, G., Mauder, M., Meier, P., Merbold, L., Mereu, S., Metzger, S., Migliavacca, M., Mölder, M., Montagnani, L., Moureaux, C., Nelson, D., Nemitz, E., Nicolini, G., Nilsson, M. B., de Beeck, M. O., Osborne, B., Löfvenius, M. O., Pavelka, M., Peichl, M., Peltola, O., Pihlatie, M., Pitacco, A., Pokorný, R., Pumpanen, J., Ratié, C., Rebmann, C., Roland, M., Sabbatini, S., Saby, N. P. A., Saunders, M., Schmid, H. P., Schrumpf, M., Sedlák, P., Ortiz, P. S., Siebicke, L., Šigut, L., Silvennoinen, H., Simioni, G., Skiba, U., Sonnentag, O., Soudani,

K., Soulé, P., Steinbrecher, R., Tallec, T., Thimonier, A., Tuittila, E.-S., Tuovinen, J.-P., Vestin, P., Vincent, G., Vincke, C., Vitale, D., Waldner, P., Weslien, P., Wingate, L., Wohlfahrt, G., Zahniser, M., and Vesala, T.: Towards long-term standardised carbon and greenhouse gas observations for monitoring Europe's terrestrial ecosystems: a review, Int. Agrophys., 32, 439–455, https://doi.org/10.1515/intag-2017-0039, 2018.

Gloor, M., Bakwin, P., Hurst, D., Lock, L., Draxler, R., and Tans, P.: What is the concentration footprint of a tall tower?, J. Geophys. Res., 106D, 17831–17840, https://doi.org/10.1029/2001JD900021, 2001.

Grimmond, C. S. B., King, T. S., Cropley, F. D., Nowak, D. J., and Souch, C.: Local-scale fluxes of carbon dioxide in urban environments: methodological challenges and results from Chicago, Environ. Pollut., 116, S243–S254, https://doi.org/10.1016/s0269-7491(01)00256-1 2002.

Haszpra, L., Barcza, Z., Bakwin, P. S., Berger, B. W., Davis, K. J., and Weidinger, T.: Measuring system for the long-term monitoring of biosphere/atmosphere exchange of carbon dioxide, J. Geophys. Res., 106D, 3057–3070, https://doi.org/10.1029/2000JD900600, 2001.

Haszpra, L., Barcza, Z., Davis, K. J., and Tarczay, K.: Long term tall tower carbon dioxide flux monitoring over an area of mixed vegetation, Agr. Forest Meteorol., 132, 58–77, https://doi.org/10.1016/j.agrformet.2005.07.002, 2005.

Haszpra, L., Hidy, D., Taligás, T., and Barcza, Z.: First results of tall tower based nitrous oxide flux monitoring over an agricultural region in Central Europe, Atmos. Environ., 176, 240–251, https://doi.org/10.1016/j.atmosenv.2017.12.035, 2018.

Haszpra, L., Ferenczi, Z., and Barcza, Z.: Estimation of greenhouse gas emission factors based on observed covariance of CO$_2$, CH$_4$, N$_2$O and CO mole fractions, Environmental Sciences Europe, 31, 95, https://doi.org/10.1186/s12302-019-0277-y, 2019.

Heidbach, K., Schmid, H. P., and Mauder, M.: Experimental evaluation of flux footprint models, Agr. Forest Meteorol., 246, 142–153, https://doi.org/10.1016/j.agrformet.2017.06.008, 2017.

Hoffer, A., Jancsek-Turóczi, B., Tóth, Á., Kiss, G., Naghiu, A., Levei, E. A., Marmureanu, L., Machon, A., and Gelencsér, A.: Emission factors for PM$_{10}$ and polycyclic aromatic hydrocarbons (PAHs) from illegal burning of different types of municipal waste in households, Atmos. Chem. Phys., 20, 16135–16144, https://doi.org/10.5194/acp-20-16135-2020, 2020.

Holtslag, A. A. M. and Nieuwstadt, F. T. M.: Scaling the atmospheric boundary layer, Bound.-Lay. Meteorol., 36, 201–209, https://doi.org/10.1007/bf00117468, 1986.

Hungarian Central Statistical Office: Gazetteer of Hungary, 1 January 2019, https://www.ksh.hu/docs/hun/hnk/hnk_2019.pdf (last access: 15 April 2020), 2019.

IPCC: 2006 IPCC Guidelines for National Greenhouse Gas Inventories – Prepared by the National Greenhouse Gas Inventories Programme, edited by: Eggleston, H. S., Buendia, L., Miwa, K., Ngara, T., and Tanabe, K., Institute for Global Environmental Strategies (IGES), Hayama, Japan, on behalf of the IPCC, ISBN 4-88788-032-4, https://www.ipcc-nggip.iges.or.jp/public/2006gl/ (last access: 26 August 2021), 2006.

IPCC: Climate Change 2014: Impacts, Adaptation, and Vulnerability. Part A: Global and Sectoral Aspects. Contribution of Working Group II to the Fifth Assessment Report of the Intergovernmental Panel on Climate Change, edited by: Field, C. B., Barros,

V. R., Dokken, D. J., Mach, K. J., Mastrandrea, M. D., Bilir, T. E., Chatterjee, M., Ebi, K. L., Estrada, Y. O., Genova, R. C., Girma, B., Kissel, E. S., Levy, A. N., MacCracken, S., Mastrandrea, P. R., and White, L. L., Cambridge University Press, Cambridge, United Kingdom and New York, NY, USA, ISBN 978-1-107-05807-1, 2014.

IPCC: 2019 Refinement to the 2006 IPCC Guidelines for National Greenhouse Gas Inventories, edited by: Calvo, B. E., Tanabe, K., Kranjc, A., Baasansuren, J., Fukuda, M., Ngarize, S., Osako, A., Pyrozhenko, Y., Shermanau, P., and Federici, S., IPCC, Switzerland, ISBN 978-4-88788-232-4, 2019.

Kljun, N., Rotach, M. W., and Schmid, H. P.: A Three-Dimensional Backward Lagrangian Footprint Model For A Wide Range Of Boundary-Layer Stratifications, Bound.-Lay. Meteorol., 103, 205–226, https://doi.org/10.1023/A:1014556300021, 2002.

Kljun, N., Calanca, P., Rotach, M. W., and Schmid, H. P.: A Simple Parameterisation for Flux Footprint Predictions, Bound.-Lay. Meteorol., 112, 503–523, https://doi.org/10.1023/B:BOUN.0000030653.71031.96, 2004a.

Kljun, N., Kastner-Klein, P., Fedorovich, E., and Rotach, M. W.: Evaluation of Lagrangian footprint model using data from wind tunnel convective boundary layer, Agr. Forest Meteorol., 127, 189–201, https://doi.org/10.1016/j.agrformet.2004.07.013, 2004b.

Kljun, N., Calanca, P., Rotach, M. W., and Schmid, H. P.: A simple two-dimensional parameterisation for Flux Footprint Prediction (FFP), Geosci. Model Dev., 8, 3695–3713, https://doi.org/10.5194/gmd-8-3695-2015, 2015 (code available at: https://footprint.kljun.net/, last access: 8 October 2020).

Magyar Közút: Az országos közutak 2018, évre vonatkozó keresztmetszeti forgalma, https://internet.kozut.hu/kozerdeku-adatok/orszagos-kozuti-adatbank/forgalomszamlalas/ (last access: 15 April 2020), 2019.

Moran, D., Kanemoto, K., Jiborn, M., Wood, R., Többen, J., and Seto, K. C.: Carbon footprints of 13 000 cities, Environ. Res. Lett., 13, 064041, https://doi.org/10.1088/1748-9326/aac72a, 2018.

Oettl, D.: Evaluation of the Revised Lagrangian Particle Model GRAL against wind-tunnel and field observations in the presence of obstacles, Bound.-Lay. Meteorol., 155, 271–287, https://doi.org/10.1007/s10546-014-9993-4, 2015a.

Oettl, D.: Quality assurance of the prognostic, microscale wind-field model GRAL 14.8 using wind-tunnel data provided by the German VDI guideline 3783-9, J. Wind Eng. Ind. Aerod., 142, 104–110, https://doi.org/10.1016/j.jweia.2015.03.014, 2015b.

Oettl, D., Sturm, P. J., Bacher, M., Pretterhofer, G., and Almbauer, R. A.: A simple model for the dispersion of pollutants from a road tunnel portal, Atmos. Environ., 36, 2943–2953, https://doi.org/10.1016/S1352-2310(02)00254-6, 2002.

Papale, D.: Ideas and perspectives: enhancing the impact of the FLUXNET network of eddy covariance sites, Biogeosciences, 17, 5587–5598, https://doi.org/10.5194/bg-17-5587-2020, 2020.

Rana, G., Martinelli, N., Famulari, D., Pezzati, F., Muschitiello, C., and Ferrara, R. M.: Representativeness of carbon dioxide fluxes measured by eddy covariance over a Mediterranean urban district with equipment setup restrictions, Atmosphere, 12, 197, https://doi.org/10.3390/atmos12020197, 2021.

Romanov, A. A., Gusev, B. A., Leonenko, E. V., Tamarovskaya, A. N., Vasiliev, A. S., Zaytcev, N. E., and Philippov, I.

K.: Graz Lagrangian Model (GRAL) for pollutants tracking and estimating sources partial contributions to atmospheric pollution in highly urbanized areas, Atmosphere, 11, 1375, https://doi.org/10.3390/atmos11121375, 2020.

Satar, E., Berhanu, T. A., Brunner, D., Henne, S., and Leuenberger, M.: Continuous CO_2 / CH_4 / CO measurements (2012–2014) at Beromünster tall tower station in Switzerland, Biogeosciences, 13, 2623–2635, https://doi.org/10.5194/bg-13-2623-2016, 2016.

Schmid, H. P.: Source areas for scalars and scalar fluxes, Bound.-Lay. Meteorol., 67, 293–318, 1994.

Stagakis, S., Chrysoulakis, N., Spyridakis, N., Feigenwinter, C., and Vogt, R.: Eddy Covariance measurements and source partitioning of CO_2 emissions in an urban environment: Application for Heraklion, Greece, Atmos. Environ., 201, 278–292, https://doi.org/10.1016/j.atmosenv.2019.01.009, 2019.

Tanács, E., Belényesi, M., Lehoczki, R., Pataki, R., Petrik, O., Standovár, T., Pásztor, L., Laborczi, A., Szatmári, G., Molnár, Z., Bede-Fazekas, Á., Kisné Fodor, L., Varga, I., Zsembery, Z., and Maucha, G.: Országos, nagyfelbontású ökoszisztéma-alaptérkép: módszertan, validáció és felhasználási lehetőségek (A national, high-resolution ecosystem basemap: methodology, validation, and possible uses), Természetvédelmi Közlemények, 25, 34–58, https://doi.org/10.20332/tvk-jnatconserv.2019.25.34, 2019.

Technische Universität Graz: GRAL – Graz Lagrangian Model, Technische Universität Graz [code], https://gral.tugraz.at/index.php/download, last access: 1 November 2021.

Tian, H., Xu, R., Canadell, J. G., Thompson, R. L., Winiwarter, W., Suntharalingam, P., Davidson, E. A., Ciais, P., Jackson, R. B., Janssens-Maenhout, G., Prather, M. J., Regnier, P., Pan, N., Pan, S., Peters, G. P., Shi, H., Tubiello, F. N., Zaehle, S., Zhou, F., Arneth, A., Battaglia, G., Berthet, S., Bopp, L., Bouwman, A. F., Buitenhuis, E. T., Chang, J., Chipperfield, M. P., Dangal, S. R. S., Dlugokencky, E., Elkins, J. W., Eyre, B. D., Fu, B., Hall, B., Ito, A., Joos, F., Krummel, P. B., Landolfi, A., Laruelle, G. G., Lauerwald, R., Li, W., Lienert, S., Maavara, T., MacLeod, M., Millet, D. B., Olin, S., Patra, P. K., Prinn, R. G., Raymond, P. A., Ruiz, D. J., van der Werf, G. R., Vuichard, N., Wang, J., Weiss, R. F., Wells, K. C., Wilson, C., Yang, J., and Yao, Y.: A comprehensive quantification of global nitrous oxide sources and sinks, Nature, 586, 248–256, https://doi.org/10.1038/s41586-020-2780-0, 2020.

van der Kwast, J., Timmermans, W., Gieske, A., Su, Z., Olioso, A., Jia, L., Elbers, J., Karssenberg, D., and de Jong, S.: Evaluation of the Surface Energy Balance System (SEBS) applied to ASTER imagery with flux-measurements at the SPARC 2004 site (Barrax, Spain), Hydrol. Earth Syst. Sci., 13, 1337–1347, https://doi.org/10.5194/hess-13-1337-2009, 2009.

Vesala, T., Kljun, N., Rannik, Ü., Rinne, J., Sogachev, A., Markkanen, T., Sabelfeld, K., Foken, T., and Leclerc, M. Y.: Flux and concentration footprint modelling: State of the art, Environ. Pollut., 152, 653–666, https://doi.org/10.1016/j.envpol.2007.06.070, 2008.

Vogt, R., Christen, A., Rotach, M. W., Roth, M., and Satyanarayana, A. N. V.: Temporal dynamics of CO_2 fluxes and profiles over a Central European city, Theor. Appl. Climatol., 84, 117–126, https://doi.org/10.1007/s00704-005-0149-9, 2006.

WMO: 20th WMO/IAEA Meeting on Carbon Dioxide, Other Greenhouse Gases and Related Measurement Techniques (GGMT-2019), Jeju Island, South Korea, 2–5 September 2019, edited by: Crotwell, A., Lee, H., and Steinbacher, M., GAW Report No. 255, https://library.wmo.int/doc_num.php?explnum_id=10353 (last access: 29 August 2022), 2020.

Zheng, B., Chevallier, F., Yin, Y., Ciais, P., Fortems-Cheiney, A., Deeter, M. N., Parker, R. J., Wang, Y., Worden, H. M., and Zhao, Y.: Global atmospheric carbon monoxide budget 2000–2017 inferred from multi-species atmospheric inversions, Earth Syst. Sci. Data, 11, 1411–1436, https://doi.org/10.5194/essd-11-1411-2019, 2019.